Electronic Supplementary Information

Tunable *in-plane* thermal conductivity in single PEDOT:PSS nanotube

Hye Jeong Lee[a], Hosun Shin[b], Gopinathan Anoop[a], Tae Jin Yoo[a], Soon Sung So[a], Jeongjae Ryu[c], Byoung Hun Lee[a], Jae Yong Song[b], Eunji Lee[a], Seungbum Hong[c], Joo-Hyoung Lee[a] and Ji Young Jo[a*]

[a] School of Materials Science and Engineering, Gwangju Institute of Science and Technology, Gwangju 61005, Republic of Korea. E-mail: jyjo@gist.ac.kr
[b] Center for Convergence Property Measurement, Korea Research Institute of Standards and Science, Daejeon 34113, Republic of Korea.
[c] Department of Materials Science and Engineering, Korea Advanced Institute of Science and Technology, Daejeon 34141, Republic of Korea.

1. Experimental section

Materials

The PEDOT:PSS (Clevios, PH1000) solution with 5 vol% of dimethyl sulfoxide (DMSO) was mixed for 24 h at room temperature after filtering. A syringe filter with a pore size of 0.45 μm was used to remove large particles for the infiltration process. Anodic Aluminum Oxide (AAO) with a 200 nm pore size template for the solution infiltration is purchased from the Bonding Chemical.

Infiltration process

At first, the PEDOT:PSS solution was dropped on to the AAO template and PEDOT:PSS solution was infiltrated into the AAO template for 24 h at room temperature. Then the sample was baked at 120^{o}C to remove residual solvent followed by Ethylene glycol (EG) or sulfuric acid (H_2SO_4) treatment for 120 min or 10 min, respectively, for improving the electrical properties of PEDOT:PSS nanotubes. The samples were then rinsed and then baked at 120^{o}C for 10 min. The AAO barrier layer was removed by immersing the template in NaOH followed by vacuum filtering using porous oxide filter paper (pore size 0.2 μm, Whatman Anodisc) for low van der Waals forces between nanotube and substrate. The PEDOT:PSS nanotubes were then collected and transfer the various substrates using Picoprobe T-4-10 with point radius of 0.1 μm or less

Characterization

SEM images were measured by FE-SEM(S-4800, by Hitachi STEM), and Raman analysis was carried out using a Raman microscope (RENISHAW, inVia) with an excitation wavelength of 514 nm.

For the AFM measurements, we used a commercial AFM (Asylum, MFP-3D) equipped with the standard ORCA module featuring dual gain current detection. All analyses were carried out under ambient conditions. The PtIr5-coated probe (Nanoworld, EFM) with a spring constant ~2.8 N/m and a tip radius of less than 25 nm was used. In the AC mode, free vibration amplitude and setpoint amplitudes were 50 nm and 30 nm, respectively. The scan size was 5 μm × 5 μm. The scan rate was set as 0.2 Hz to prevent the nanotubes from slipping. After the AC mode scanning, we performed I-V spectroscopy to characterize the resistance of fabricated PEDOT:PSS nanotubes using the conductive AFM (C-AFM) mode. The Au-coated Si substrates were electrically connected to a metal plate with

Ag paste. The voltage with a frequency of 1 Hz was applied to the metal plate. The applied force was 500 nN during the I-V characterization. When imaging in the non-contact mode, the AFM tip did not indent deeper than the wall thickness of NTs (65 nm).

Thermal conductivities for PEDOT:PSS nanotubes were measured using the suspended microstructure[18,19], which is fabricated with 500 nm thick low-stress silicon nitride deposited on a silicon wafer using a lithography method. A Pt nanopattern, including a nano-heater and a pair of thermometers, were formed on the suspended silicon nitride. The temperature coefficient of resistance (TCR) of the Pt thermometers were used in order to determine the temperature at two thermometers, which was done by converting the resistance change (ΔR) to the temperature change (ΔT) with the TCR values in the temperature range of 240 K to 400 K under 10^{-6} Torr vacuum condition. [Details of device fabrication and measurement are described in the ref.1]

Simulation details

Generally, the simulations for polymers are computationally more time-consuming than typical all-atom molecular dynamics (AAMD) simulations because the monomers constituting polymers usually have more than two atoms, resulting in much longer simulations. For this kind of restricted situations, instead of using the all-atom scheme, we adopted coarse-grained (CG) MD simulation that considers the several atoms to one bead leading to extending to the larger scale.[3]

While there are several CG force fields, such as CHARMM, GROMOS, and MARTINI [4–7] have been developed, for the computational efficiency, we followed a simplified CG model potential and optimized parameters for PEDOT:PSS (Figure S5).[8]

For the models used in this work, although it was from ref. 6 for describing the PEDOT:PSS films, there are still several conflicting reports on morphologies of PEDOT:PSS [7,] and furthermore any proper tube models are not reported to the best of our knowledge. So it was inevitable that we assume the structures on calculations that rather be ideal than reported cases, and therefore, we aligned the chains crossed for films and paralleled for tubes, respectively (FigureS5).

The thermal conductivity of PEDOT:PSS tubes and PEDOT:PSS films in the length direction (D_L) was obtained using the reverse non-equilibrium molecular dynamics (RNEMD) [9] simulations packaged in LAMMPS [10].

In the RNEMD, the heat flux J is imposed on the simulation cell by exchanging the energy of atoms in cold slab located at the end to that of the hot slab in the middle of the cell. The transferred energies of the hottest atoms in cold slab and the coldest atoms in the hot slab make hot slab hotter and cold slab colder, respectively, and this difference makes the heat flux in the cell after any time t, given by

Eq1.

$$J = -\frac{\sum_{transter} (E_k^{hot} - E_k^{cold})}{2tS}$$

where E_k^{hot} and E_k^{cold} are the exchanged kinetic energies of the hot slab and cold slab, respectively, and S is the cross-sectional area. Factor 2 considered the fact that the heat flow propagated to both cold ends. After then, the balance between artificial energy exchanges and the heat flux in the opposite direction is established, and the cell thermally reaches steady states. The obtained temperature profile is used directly to compute the thermal conductivity via the equation known as Fourier's law,

Eq2.

$$\kappa = -\frac{J}{\nabla T} = \lim_{\nabla T \to 0} \lim_{t \to \infty} -\frac{\langle J(t) \rangle}{\langle \partial T / \partial z \rangle}$$

where the ∇T is the temperature gradient of the simulation cell, and the brackets indicate the ensemble average of the quantities over time.

Each slab in the cell has approximately 1nm width in the temperature profiles. It must be careful to choose the regimes in temperature profile due to the existence of hot and cold slabs in RNEMD that causes the nonlinear effect so the Fourier's law cannot be described appropriately. Thus, we picked the positions of 1/10L, 4/10L, 6/10L, and 9/10L where it is enough to avoid the nonlinearity, and used the slopes to compute the κ.

The systems ranging from 240 to 400K are relaxed under a constant volume and constant temperature (NVT) ensemble using Nosé-Hoover thermostat with a time step of 5 fs over the 5 ns and then followed by microcanonical ensemble (NVE) with a time step of 1 fs over the 2 ns so that the total energy of the system was conserved. After that, the temperature profile was computed over 1 ns along the length direction.

Considering the restricted condition of size and the stable simulations, the periodic boundary condition was applied to all directions for the films and to only length directions for tubes. In addition, after tests for D_{PSS} from 10 to 20 nm for the film model, we chose a width of 20 nm for stable RNEMD simulation. The $\kappa$of each of models for infinite length was calculated from 80 nm up to 400 nm by plotting inverse κ as a function of inverse sample length using the following equation [11]

Eq3.

$$\frac{1}{\kappa} = \frac{a}{L_z} + \frac{1}{\kappa_\infty}$$

where κ is the thermal conductivity in a data with a finite length, a is a factor related to the effective phonon mean free path, L_z is the length in the z-direction, and κ_∞ is the thermal conductivity of an infinitely long model.

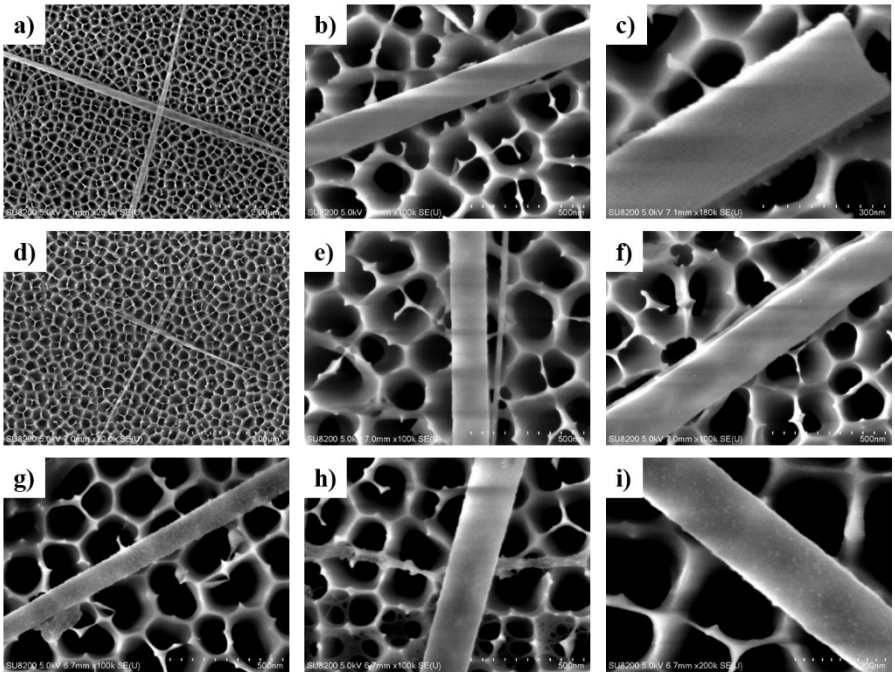

Figure S1. The SEM images of PEDOT:PSS nanotubes on oxide filters. (a)-(c) pristine, (d)-(e) EG-treated, (g)-(i) H2SO4-treated samples, respectively.

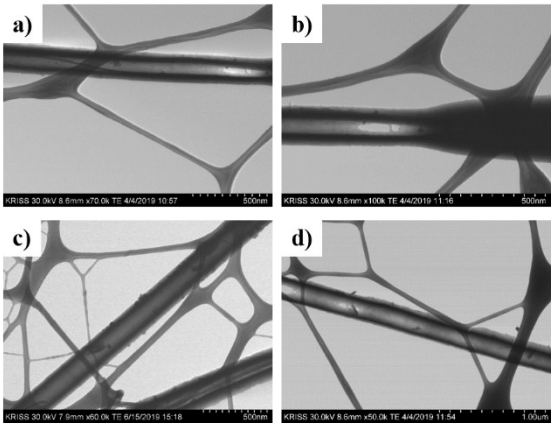

Figure S2. STEM images of PEDOT:PSS nanotube in (a) low and (b) high resolutions for the pristine sample. (c) EG-treated and (d) H_2SO_4-treated sample

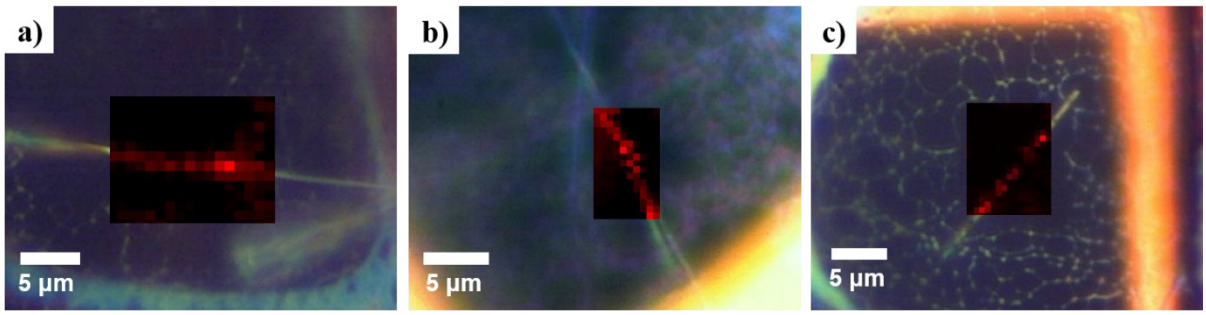

Figure S3. Raman mapping images of PEDOT:PSS nanotubes. (a) pristine sample. (b) EG-treated and (c) H_2SO_4-treated sample

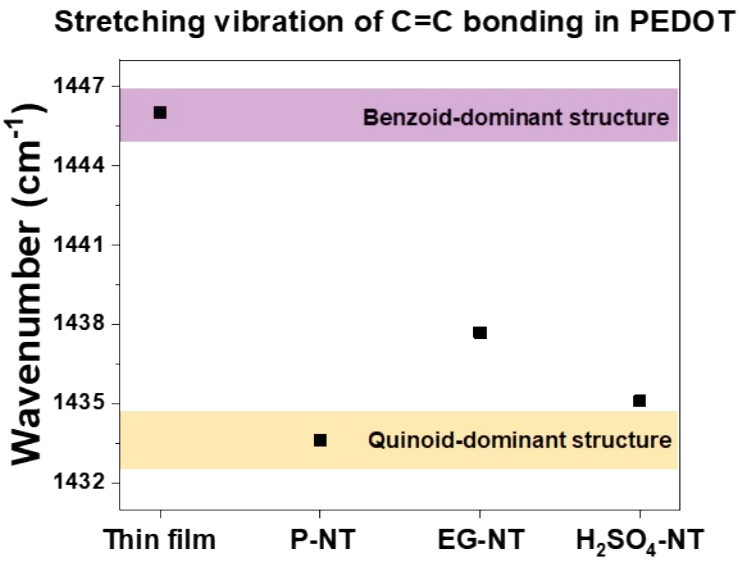

Figure S4. The $C_\alpha = C_\beta/C_\alpha - C_\beta$ vibration peak of the thin film, P-NT, EG-NT, and H_2SO_4-NT.

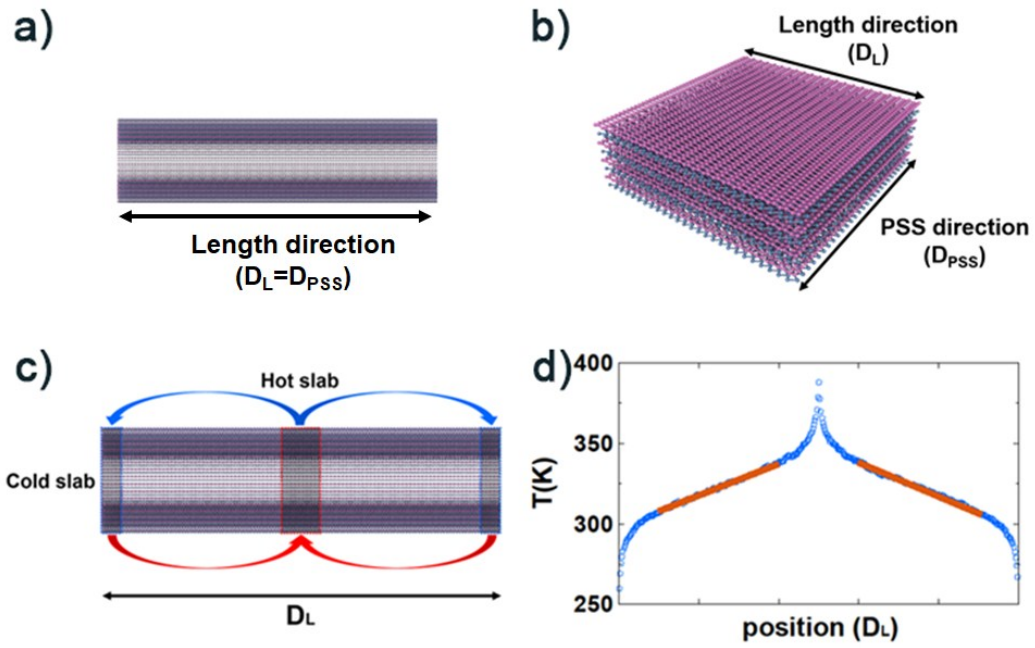

Figure S5. We denoted each length as D_L and D_{PSS}, respectively. a) All polymer chains are aligned in length direction (b). The PEDOT chains and PSS chains in the film model aligned to be crossed. We denoted each length as D_L and D_{PSS}, respectively. c) and d) Typical temperature profile and schematic picture in PEDOT:PSS tube along the length direction. In RNEMD, exchanging the energy of atoms in cold slab located at both ends to that of the hot slab at the middle of the cell forms heat flux.

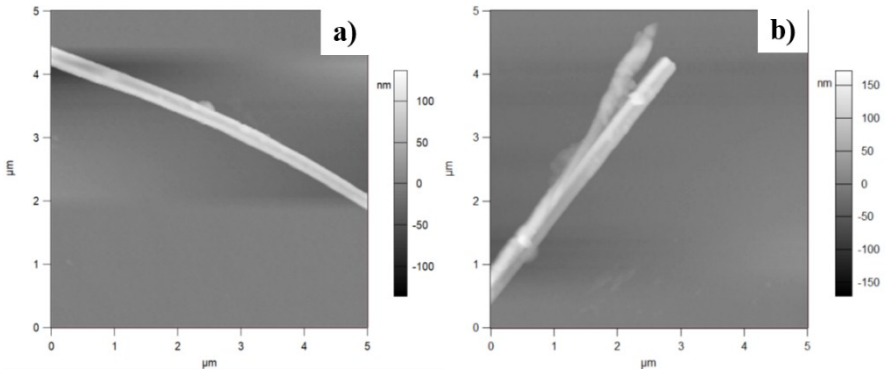

Figure S6. AFM images of PEDOT:PSS nanotubes transferred onto a gold-coated silicon substrate. (a) pristine and (b) H_2SO_4-treated sample.

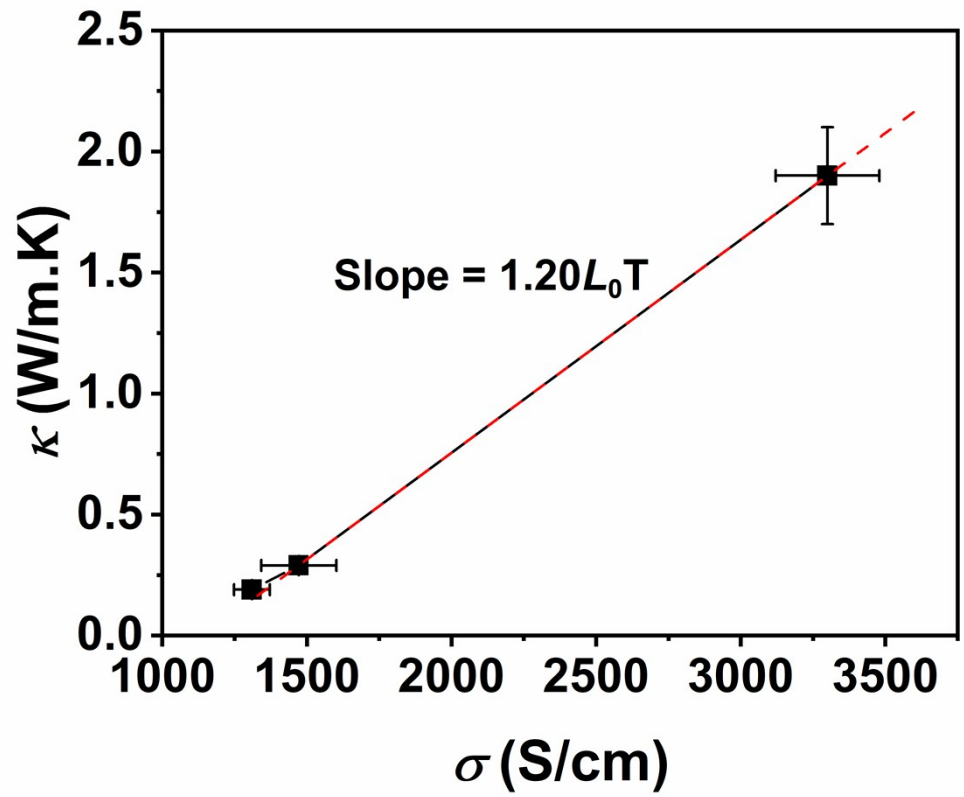

Figure S7. κ–σ plot of pristine, EG, and H_2SO_4-treated PEDOT:PSS. The slope of the fitted line is around 1.20L_0T.

References

(1) H. S. Shin, S. G. Jeon, J. Yu, Y.-S. Kim, H. M. Park and J. Y. Song, *Nanoscale*, 2014, **6**, 6158–6165.

(2) S. G. Jeon, D. W. Park, H. S. Shin, H. M. Park, S. Y. Choi, S. J. Lee, J. Yu and J. Y. Song, *RSC Adv.*, 2016, **6**, 7791–7797.

(3) Marrink, S. J.; De Vries, A. H.; Mark, A. E. *J. Phys. Chem. B* 2004, **108** (2), 750–760.

(4) Brooks, B. R.; Brooks, C. .; Mackerell, A. D.; Nilsson, L.; Petrella, R. J.; Roux, B.; Won, Y.; Archontis, G.; Bartels, C.; Boresch, S.; Caflisch, A.; Caves, L.; Cui, Q.; Dinner, A. R.; Feig, M.; Fischer, S.; Gao, J.; Hodoscek, M.; Im, W.; Kuczera, K.; Lazaridis, T.; Ma, J.; Ovchinnikov, V.; Paci, E.; Pastor, R. W.; Post, C. B.; Pu, J. Z.; Schaefer, M.; Tidor, B.; Venable, R. M.; Woodcock, H. L.; Wu, X.; Yang, W.; D.M, Y.; Karplus, M. *J. Comput. Chem.* 2009, **30**, 1545–1614.

(5) Reif, M. M.; Hünenberger, P. H.; Oostenbrink, C. *J. Chem. Theory Comput.* 2012, **8**, 3705–3723.

(6) Marrink, S. J.; Tieleman, D. P. *Chem. Soc. Rev.* 2013, **42**, 6801–6822.

(7) Modarresi, M.; Franco-Gonzalez, J. F.; Zozoulenko, I. *Phys. Chem. Chem. Phys.* 2019, **21**, 6699–6711.

(8) Lee, C. K.; Wodo, O.; Ganapathysubramanian, B.; Pao, C. W. *ACS Appl. Mater. Interfaces* 2014, **6**, 20612–20624.

(9) Müller-Plathe, F. *J. Chem. Phys.* 1997, *106* (14), 6082–6085.

(10) Plimpton, S. *J. Comput. Phys.* 1995, **117**, 1–19.

(11) Schelling, P. K.; Phillpot, S. R.; Keblinski, P. *Phys. Rev. B* 2002, **65**, 144306.